ENERGY CONSERVATION AND HEAT TRANSFER ENHANCEMENT FOR MIXED CONVECTION ON THE VERTICAL GALVANIZING FURNACE

by

Dan MEI[a,c], Yuzheng ZHU[a], Xuemei XU[a], and Futang XING[a,b*]

[a] Hubei Provincial Industrial Safety Engineering Technology Research Center, Wuhan University of Science and Technology, Wuhan, Hubei, China
[b] Hubei Key Laboratory of Ind Fume and Dust Pollution Control, Jianghan University, Hubei, China
[c] Department of Mechanical and Aerospace Engineering, Old Dominion University, Norfolk Va., USA

Original scientific paper
https://doi.org/10.2298/TSCI180105180M

The alloying temperature is an important parameter that affects the properties of galvanized products. The objective of this study is to explore the mechanism of conjugate mixed convection in the vertical galvanizing furnace and propose a novel energy conservation method to improve the soaking zone temperature based on the flow pattern and heat transfer characteristics. Herein, the present study applied the k-ε two-equation turbulence model to enclose the Navier-Stokes fluid dynamic and energy conservation equations, and the temperature distributions of the steel plate and air-flow field in the furnace were obtained for six Richardson numbers between $1.91 \cdot 10^5$ and $6.30 \cdot 10^5$. In the industrial practice, the side baffles were installed at the lateral opening of the cooling tower to alter the height of vertical flow passage, which affected the Richardson number. The results indicate that the Richardson number of $2.4 \cdot 10^5$ generated the highest heat absorption and maximal temperature in the steel plate due to the balance between natural and forced convection. Furthermore, the results of the on-line experiments validated the simulation research. The method enhanced the steel plate temperature in the soaking zone without increasing the heat power, thereby characterizing it as energy conservation technology.

Key words: *energy conservation, vertical galvanizing furnace, heat transfer, mixed convection, numerical simulation*

Introduction

Hot-dip galvanized steel is a strip coated zinc-iron alloy produced by hot dipping and the on-line annealing treatment. It is applied in the automobile industry due to its advanced corrosion resistance, high strength, and outstanding welding properties.

The hot-dip galvanized treatment is conducted in the vertical alloying furnace, which is divided into three parts from the bottom to the roof: the mobile soaking zone, fix soaking zone, and cooling tower, respectively, as presented in fig. 1. After its removal from the zinc bath, the steel sheet enters the soaking zone, wherein the zinc layer and steel substrate are heated by electromagnetic induction meet the alloying treatment demand. In the soaking zone,

* Corresponding author, e-mail: meidan@wust.edu.cn

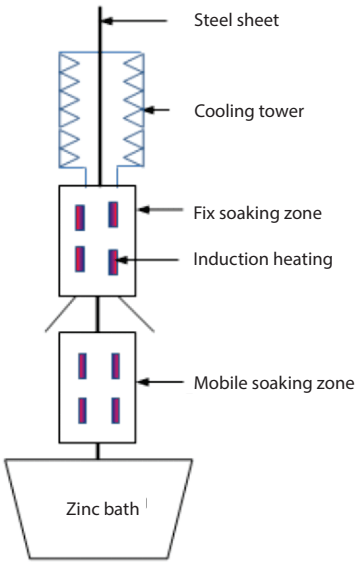

Figure 1. Sketch map of the galvanizing furnace

the hot galvanized steel sheet is generated by diffusion and reaction between zinc layer and steel substrate. The sheet is then cooled by forced convection in the cooling tower with jets [1].

During the thermal treatment, it is essential that the hot-dip galvanized steel sheet be heated rapidly, completely, and uniformly along the width direction generate high-quality galvanized steel sheets. In general, the temperature in the soaking zone can be enhanced to achieve uniform and efficient heating by: increasing the heat flux [2] and adding regulating pressure fans and air-sealed devices on the top of the soaking zone to reduce heat loss. These measures generate qualified thermal treatment but correspondingly increase the required energy input and production cost, thereby reducing the energy efficiency of the production process.

Variations of geometrical factors have been regarded as an effective way to enhance thermal performance without increasing the alloying energy input requirements [3]. The thermal process in an industrial furnace is related to non-isothermal, incompressible gas-solid turbulent flow. Numerical simulations can reveal the distribution of flow and temperature field in the furnace and has been widely used in the design and research of industrial furnaces. El-Kaddah [4] established 3-D flow and temperature distribution characteristics of induction heating in a steel sheet rolled process based on the numerical simulations, and Veranth [5] acquired the temperature distribution of a rotary kiln in the treatment of industrial waste residue. Mastorakos [6] established the mathematical model of cement kiln and performed numerical calculations on the combustion and heat transfer in the pits. Moon [7] performed numerical simulations on the full-hydrogen furnace annealing process, thereby obtaining the laws that governed the circulatory air volume and annealing time.

A steel plate moves vertically upward in an alloying furnace. Its lower part is heated by electromagnetic induction in the soaking zone, and its upper part is cooled by low temperature spray air in the cooling zone, which can be regarded as the vertical motion of a big plate with limited space and mixed convection in consideration of its heating and cooling sources. Mixed convection in finite channels occurred in numerous applications, such as solar systems [8], conventional flat plate collectors [9], and heat exchangers [10]. These studies used theoretical analysis [11], experiments [12] and calculations [13-15] to assess the effects of the Reynolds and Richardson numbers on the convection and heat transfer in terms of their respective assistance or opposition buoyancy and in consideration of cases that exhibited heating with high temperature or heat fluxes.

The Richardson number, which is also known as the buoyancy parameter is employed to assess the comparison of the natural-convection and the forced convection [16], defined as $\mathrm{Ri} = (g\beta\Delta t H^3)/(4d^2u_0^2)$. Garoosi, *et al*. [17] concerned heat transfer of free and mixed convection in a square cavity fixed several heat source-sinks. Effects of some governing parameters such as Richardson number on the heat transfer rates were investigated. Patil, *et al*., [18] studied steady 2-D double diffusive mixed convection along a vertical semi-infinite permeable surface. Results have indicated that buoyancy parameter, Ri, and the ratio of buoyancy forces parameter

enhanced the skin friction coefficient and decreased the heat transfer coefficient. Mehrizi, *et al.* [19] carried out numerical simulation of mixed-convection heat transfer in a horizontal ventilated cavity with a thin partition on the bottom heated surface. They concluded that increase in Richardson number resulted in reduction of average Nusselt number. Mahmoodi [20] investigated numerically mixed convection fluid-flow and heat transfer in lid-driven rectangular enclosures. A parametric study was performed and the effects of the Richardson number on heat transfer inside the enclosure were investigated. The results shown that at low Richardson numbers, a primary counterclockwise vortex was formed inside the enclosure. Therefore, regulation of Richardson number can enhance heat transfer of mixed convection.

In this research, a numerical simulation was established to characterize the mixed convection in the alloying furnace as well as the effect of the Richardson number on the heat transfer and average Nusselt number. Regarding the flow field characteristic, an energy conservation method was generated to optimize the flow field structure without increasing the heating power, thereby fulfilling the temperature requirements and ensuring the quality of the hot-dip galvanized steel sheets.

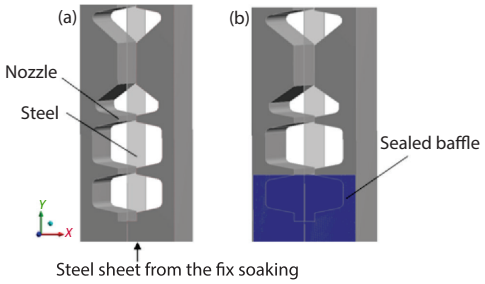

Figure 2. The 3-D schematic diagram of segmental cooling tower; (a) original cooling tower, (b) adding the sealed baffle on the opening

Models and methods

The 3-D schematic diagram of segmental cooling tower of the vertical galvanizing furnace is presented in the fig. 2. The hot air-flow rose from the soaking zone due to the buoyancy effect and overflows at the opening, which caused heat dissipation and changed the temperature in the soaking zone from fulfilling the design requirements. To achieve thermal preservation, the openings at the junction of soaking and cooling zone were partially sealed to reduce the heat loss caused by hot air overflowing. The technical measure practiced at the industry line is presented in fig. 2(b). The presented heat transfer enhancement and mixed convection mechanisms were interpreted by computational simulation and the precise heights of the sealed baffles were validated by online experiments.

Geometry model

From the viewpoint of the numerical simulation, the computational domain of the galvanizing furnace which contains steel sheet and air-flow is illustrated in fig. 3. The vertical direction is set as the *Y*-axis, and the normal of the steel plate is set as the *X*-axis. The heating and soaking zone had a total length of 25 m. The electromagnetic introduction re-

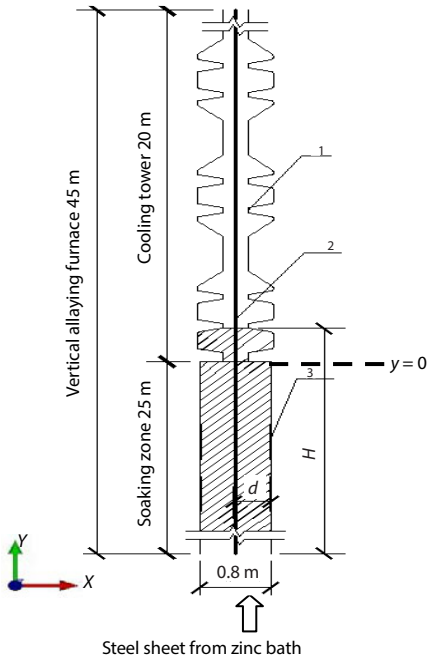

Figure 3. Sketch model of the computational domain; *1 – jet nozzles, 2 – steel sheet, 3 – induction soaking zone*

sistances were symmetrically distributed on both sides of the sheet and the width of one side was $d = 0.4$ m. The cooling tower, which was 20 m in length, had three parts, wherein each part had 14 arrays of nozzles and the height of the crack was 0.01 m. The galvanized steel sheet had a thickness of 1 mm and a width of 1.2 m. The soaking zone was enclosed while the cooling tower was opening. The roof of cooling tower was open and contacted with atmospheric air. The H is expressed as the total length of the soaking zone and the sealing baffle as presented in fig. 3.

Mathematic model

The fluid in the soaking zone and cooling tower was air. According to the pressure within the galvanizing furnace, the flow was incompressible turbulence, which was described by the Reynolds-averaged Navier-Stokes fluid dynamic equations. The researchers have previously evaluated several eddy viscosity models applied to impinging gas-jet system (IJS) [21]. Coussirat [22] imposed that the k-ε two-equation turbulence model could simulate the flow behaviors in the IJS. Mathews [23] also have used the k-ε model coupled the energy equation in analyzing heat transfer rate of a vertical passage with several thermal sources. Since the precious references have affirmed the capability of the k-ε model, the present study adopted this model to enclose the Navier-Stokes dynamic equations. The buoyancy force was considered in term of Boussinesq approximation. Convection and radiation heat transfer affect the heat flow and temperature distribution in a vertical galvanizing furnace. The temperature discrepancy between the socking zone and cooling tower resulted in convection heat transfer.

The dimensionless mass, momentum and energy equations:

$$div(\overline{u}) = 0 \tag{1}$$

$$div(\overline{uu_i}) = -\frac{1}{\rho}\frac{\partial \overline{P}}{\partial X} + \frac{1}{\mathrm{Re}}(1+v_{tn})div\left(\frac{\partial \overline{u_i}}{\partial X} + \frac{\partial \overline{u_i}}{\partial Y} + \frac{\partial \overline{u_i}}{\partial Z}\right) \tag{2}$$

$$div(\overline{uu_j}) = -\frac{1}{\rho}\frac{\partial \overline{P}}{\partial Y} + \frac{1}{\mathrm{Re}}(1+v_{tn})div\left(\frac{\partial \overline{u_j}}{\partial X} + \frac{\partial \overline{u_j}}{\partial Y} + \frac{\partial \overline{u_j}}{\partial Z}\right) + \mathrm{Ri}\overline{\theta} \tag{3}$$

$$div(\overline{uu_k}) = -\frac{1}{\rho}\frac{\partial \overline{P}}{\partial Z} + \frac{1}{\mathrm{Re}}(1+v_{tn})div\left(\frac{\partial \overline{u_k}}{\partial X} + \frac{\partial \overline{u_k}}{\partial Y} + \frac{\partial \overline{u_k}}{\partial Z}\right) \tag{4}$$

$$div\left(\overline{u\theta}\right) = \frac{1}{\mathrm{Re}}\left(\frac{\alpha^*}{\mathrm{Pr}} + \frac{v_{tn}}{\sigma_T}\right)div\left(\frac{\partial \overline{\theta}}{\partial X} + \frac{\partial \overline{\theta}}{\partial Y} + \frac{\partial \overline{\theta}}{\partial Z}\right) - \frac{1}{\mathrm{Pr}\,\mathrm{Re}} \tag{5}$$

The dimensionless turbulent kinetic energy and dissipation rate equations:

$$div(\overline{uk_n}) = \frac{1}{\mathrm{Re}}\left(1 + \frac{v_{tn}}{\sigma_k}\right)div\left(\frac{\partial k_n}{\partial X} + \frac{\partial k_n}{\partial Y} + \frac{\partial k_n}{\partial Z}\right) + P_{kn} - \varepsilon_n \tag{6}$$

$$div(\overline{u\varepsilon}) = \frac{1}{\mathrm{Re}}\left(1 + \frac{v_{tn}}{\sigma_\varepsilon}\right)div\left(\frac{\partial \varepsilon_n}{\partial X} + \frac{\partial \varepsilon_n}{\partial Y} + \frac{\partial \varepsilon_n}{\partial Z}\right) + \frac{\varepsilon_n}{k_n}\left[C_{\varepsilon 1}P_{kn} - C_{\varepsilon 2}\varepsilon_n\right] \tag{7}$$

The dimensionless variables are defined:

$$(X,Y,Z)=\frac{(x,y,z)}{d},\quad (\overline{u_i},\overline{u_j},\overline{u_k})=\frac{(u_i,u_j,u_k)}{u_0},\quad \overline{P}=\frac{(p-p_0)}{(\rho u_0^2)}$$

$$\overline{\theta}=\frac{(t-t_c)}{\Delta t},\quad k_n=\frac{k}{u_0^2},\quad \varepsilon_n=\frac{\varepsilon}{\frac{u_0^3}{d}},\quad \text{and}\quad \nu_{tn}=\frac{\nu_t}{(du_0)}$$

where (X ,Y, Z) denote Cartesian co-ordinates, ($\overline{u_i}$, $\overline{u_j}$, $\overline{u_k}$) are the air speed components in the X-, Y-, and Z-directions, respectively, u_0 [ms^{-1}] – the gas jet speedm d [m] – the distance between steel strip and the shell of the furnace along X-direction, and P [Pa] – relative pressure. A combined temperature scale [24] is applied to define $\Delta t = t_h - t_c + Qd/k_f$ based on the presence of the high temperature, t_h, cool temperature, t_c, and a heat source, Q. The characters ρ and g [ms^{-2}] are the fluid density and the gravitational acceleration, respectively, and k_f [Wm^{-1}K^{-1}] – the fluid thermal conductivity. The P, θ, k_n, ε_n, and ν_{tn} represent non-dimensional quantities.

The P_{kn} denote the non-dimensional turbulent kinetic energy:

$$P_{kn}=\frac{\nu_{tn}}{\mathrm{Re}}\left\{2\left[\left(\frac{\partial\overline{u_i}}{\partial X}\right)^2+\left(\frac{\partial\overline{u_j}}{\partial Y}\right)^2+\left(\frac{\partial\overline{u_k}}{\partial Z}\right)^2\right]+\left(\frac{\partial\overline{u_i}}{\partial Y}+\frac{\partial\overline{u_j}}{\partial X}\right)^2+\left(\frac{\partial\overline{u_i}}{\partial Z}+\frac{\partial\overline{u_k}}{\partial X}\right)^2+\left(\frac{\partial\overline{u_j}}{\partial Z}+\frac{\partial\overline{u_k}}{\partial Y}\right)^2\right\}$$

where k_n [m^{2}s^{-2}] is the calculated turbulent kinetic energy, and ε_n [s^{-1}] – the dissipation rate, ν_{tn} – the non-dimensional turbulent viscosity expressed as $\nu_{tn} = (\mathrm{Re}c_\mu k_n^2)/\varepsilon_n$.

The following constants were adoped in the study [25]:

$$\sigma_k=1,\ c_\mu=0.09,\ \mathrm{Pr}=0.85,\ c_{1\varepsilon}=1.44,\ c_{2\varepsilon}=1.92,\ \sigma_\varepsilon=1.3$$

The dimensionless controlling parameter Reynolds number referred to the hydraulic diameter of the channel and the fluid speed is defined:

$$\mathrm{Re}=\frac{2du_0}{\nu} \tag{8}$$

where ν denote the fluid kinematic viscosity.

The dimensionless controlling parameters Richardson number referred to the baffle height, temperature difference and air velocity is defined:

$$\mathrm{Ri}=\frac{\mathrm{g}\beta\Delta tH^3}{4d^2u_0^2} \tag{9}$$

where β is the thermal expansion coefficient.

The Prandtl number is calculated as $\mathrm{Pr} = \nu/\alpha$, where α – the thermal diffusivity. In our calculations, the Prandtl number was fixed at 0.7.

To distinguish the solid from the fluid in the energy equation, the thermal diffusivity ratio of solid to fluid is defined $\alpha^* = k_s(\rho C_p)_f/k_f(\rho C_p)_s$, which is unity in fluid. The C_p [Jkg^{-1}K^{-1}] – the heat capacity, subscripts s and f denote the solid and fluid, respectively.

Boundary conditions

Velocity boundary conditions. The cool air spraying velocity of the nozzles was u_0 = 25 m/s. The sheet moved upwards along Y-direction at the velocity of u = 2 m/s. These velocity values came from galvanizing production-line. The turbulent intensity of inlet and outlet were set as 5%.

Thermal boundary conditions. The steel trip was heated during electromagnetic introduction process, the source intensity of which was $Q = 900$ kW. The bottom temperature of the steel trip was $t_b = 733$ K. The temperature of cool air from the nozzles was $t_c = 283$ K. The shells of the furnace were adiabatic walls. The conjugate heat transfer condition:

$$k_s \left.\frac{\partial t_f}{\partial n}\right|_{\text{fluid}} = k_f \left.\frac{\partial t_s}{\partial n}\right|_{\text{solid}}$$

was set on the interface between the gas and the sheet strip.

Numerical analysis

The ANSYS ICEM [26] is employed to generate the 3-D structural grids for the models. The mesh independence analysis validated the presence of total 2.87 million nodes within the mesh scale. An implicit SIMPLE arithmetic was adopted to solve the equation groups, namely (1)-(7), with the boundary conditions. A high resolution scheme was employed to discretize the turbulence formulations. The high resolution scheme used the second order backward Euler scheme wherever and whenever possible and reverted to the first order backward Euler scheme when required to maintain a bounded solution. The convection and diffusion terms of equations were discretized with the first-order upwind and central difference scheme, respectively. The ANSYS CFX 16.0 [25] commercial code was used to solve all the governed equations. The under-relaxation factors for velocity, energy, and mass provided damping for the aforementioned equation set. In a steady-state calculation, the default value of 0.75 has been found to be sufficiently small to dampen solutions. The convergence criteria were that the values of root mean square of residuals were below 10^{-4}.

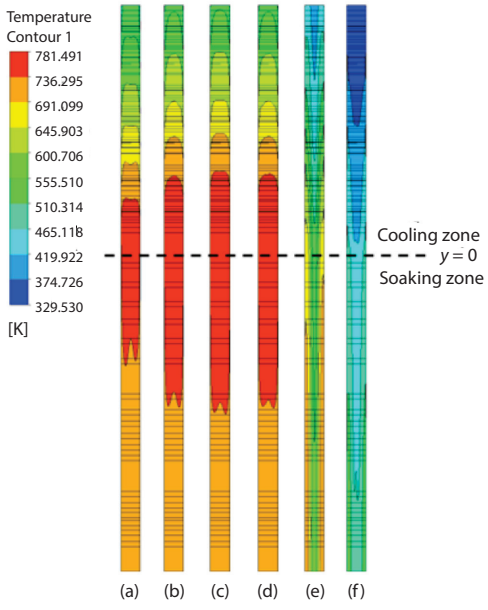

Figure 4. Isothermals of steel sheet surface at various Richardson number; (a) Ri = 1.91 · 10⁵, (b) Ri = 2.22 · 10⁵, (c) Ri = 2.30 · 10⁵, (d) Ri = 2.40 · 10⁵, (e) Ri = 3.68 · 10⁵, and (f) Ri = 6.30 · 10⁵

Results and discussion

The effects of government parameter Reynolds number on the temperature and air-flow in the galvanizing furnace have been discussed previously [27]. The effects of Richardson number were analyzed as follows. The Richardson number was varied within the range of $1.91 \cdot 10^5$-$6.30 \cdot 10^5$ by changing the baffle height at a Reynolds number fixed of $1.3 \cdot 10^6$. The height of the sealing baffles was taken as 0 m (original design structure, not sealed), 1.291 m (sealed one section of the cooling zone), 1.595 m, 1.984 m, 6.130 m (sealed two sections of the cooling zone), and 12.229 m, which were measured starting from the junction, $Y = 0$.

The effect of the Richardson number on the temperature field in the galvanizing kettle

Figure 4 presents the temperature variations of the steel plate in the vertical direction under different Richardson numbers. When $\text{Ri} = 2.20 \cdot 10^5$-$2.40 \cdot 10^5$, the temperature distribution of the steel plate met the technical

requirements of the alloying galvanizing and annealing process. When Ri = $3.68 \cdot 10^5$, the temperature in the heating zone did not increase due to rapid cooling. When Ri = $6.30 \cdot 10^5$, the temperature in the cooling zone increased, but the temperature in the heating zone decreased. When Ri = $1.91 \cdot 10^5$-$2.40 \cdot 10^5$, the horizontal temperature distribution of the steel plate was uniform, which satisfied the technical requirements for uniform heating in the galvanizing process. Nevertheless, when Ri = $3.68 \cdot 10^5$-$6.30 \cdot 10^5$, the horizontal gradient of the temperature variation was larger.

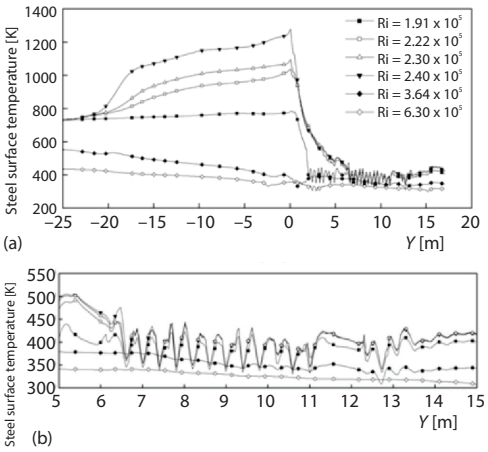

Figure 5. (a) Temperature at the central line of the steel sheet variation with *Y* at various Richardson number values, (b) detailed view at 5 m < *Y* <15 m

The temperature variations at the center axis of the steel plate with *Y* is presented in fig. 5, wherein fig. 5(b) is the magnification graph at a range of 5 m < *Y* < 15 m. The temperature variation trend at each plate section in the galvanizing furnace was more clearly compared in fig. 5. When Ri = $2.40 \cdot 10^5$, the temperature in the soaking zone was the highest. When Ri = $2.22 \cdot 10^5$-$2.40 \cdot 10^5$, the temperature exhibited the same varying trend in the cooling zones, which illustrated temperature changes due to baffle height variations in the heating zone, though this did not change the flow characteristics in the cooling zone. Each temperature oscillation corresponded to the location of nozzles in the geometry model, as presented in fig. 5(b). Therefore, cool air sprayed from the nozzles rapidly made the steel strip cool, though the temperature sharply increased in the presence of hot flow in the vertical direction.

When Ri > $3.68 \cdot 10^5$, the temperature curve exhibited a flat trend and did not conform with the production requirements of the plate temperature, which first rose and then dropped. The temperature in the soaking zone was lower than 500 K, and the temperature in the cooling zones no longer exhibited an oscillating trend, which indicate that the excessive sealed height completely changed the air-flow direction in the furnace and restricted cool air-flowing outside. As a result, the cooling effect was enhanced.

Table 1 presents the Nusselt number at the steel plate in the soaking zone under different Richardson numbers. It is defined:

$$\overline{\mathrm{Nu}} = \int_{\text{soaking zone}} \frac{\partial t}{\partial n}\Big|_{x=0} \mathrm{d}y$$

where t is the local plane temperature.

Table 1. The Nusselt number at the steel strip surface in the soaking zone

Ri	Ri = $1.91 \cdot 10^5$	Ri = $2.22 \cdot 10^5$	Ri = $2.30 \cdot 10^5$	Ri = $2.40 \cdot 10^5$	Ri = $3.68 \cdot 10^5$	Ri = $6.30 \cdot 10^5$
Nu	$-5.73 \cdot 10^{-4}$	$-1.25 \cdot 10^{-3}$	$-1.55 \cdot 10^{-3}$	$-2.01 \cdot 10^{-3}$	$2.04 \cdot 10^{-3}$	$2.54 \cdot 10^{-3}$

In the case of the original design (Ri = $1.91 \cdot 10^5$), the steel plate exhibited heat absorption. When Ri = $2.40 \cdot 10^5$, the heat absorption of the steel plate reached its maximum such that the plate temperature also rapidly increased. When the Richardson number continuously increased, the Nusselt number changed from a negative to a positive value, thereby changing the heat transfer of the steel plate from heat absorption release and reducing the overall plate temperature.

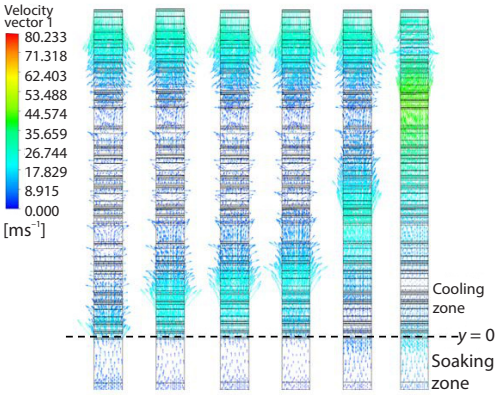

Figure 6. Air velocity vectors at various Richardson number; (a) Ri = 1.91 · 10^5 (b) Ri = 2.22 · 10^5, (c) Ri = 2.30 · 10^5, (d) Ri = 2.40 · 10^5, (e) Ri = 3.68 · 10^5, and (f) Ri = 6.30 · 10^5

The effect of the Richardson number on the air-flow in the galvanizing kettle

To understand the influence of the Richardson number on the air-flow, the fig. 6 presented air-flow velocity vector on the *Y-Z* plane, which was parallel to the steel sheet, $X = 0.06$ m. A comparison of the air velocity and flow direction under different Richardson numbers exhibited an average air-flow direction changed from upward to downward wherein an increase in the sealed height. This illustrates the presence of competition between the hot and cool air-flows at $Y = 0$. When the speed was positive, the hot gas-flow rose and natural-convection dominated. However, excessive Richardson number ($Ri \geq 3.68 \cdot 10^5$) values resulted in cool air moving down along the vertical channel due to intensive forced convection, thereby reducing the temperature of the steel sheet.

Experiment validation of the optimal sealed heights

This study implemented two simulation validation tasks to adequately validate the numerical accuracy. The first was to test the applicability of the *k-ε* turbulence model and to validate the prediction of conjugated convection heat transfer. Table 2 lists the temperature along the vertical centerline of steel strip obtained by computational simulation and measure in the production-line. The production conditions indicated a steel strip width of 1.2 m, a steel strip thickness of 0.69 mm, a steel plate vertical transport speed of 1.67 m/s, a heating power of electromagnetic induction of 900 W, and a cool air jet velocity of 25 m/s. In the experimental study, the nickel-chrome and nickel-silicon *K*-type thermocouples (WRN-130) and the temperature sensors were used to measure the plate temperature. The data were recorded every 2 minutes. The average temperatures were obtained for 50 minutes, which were displayed in the tab. 2.

Based on the data presented in tab. 2, it is accepted that the differences between the simulated study and monitored results was approximately 5%. As demonstrated in the model validation study, the numerical model and method used in this study are capable of simulating air-flow characteristic and researching conjugated convection of the vertical galvanizing furnace.

Table 2. Validation of the simulated results under the working conditions

Observation location (x, y)	(0, –24)	(0, –15)	(0, –12)	(0, –8)	(0.125, 6.1)	(0.125, 6.4)	(0.125, 12)
Simulation results [K]	730.21	767.82	781.45	804.63	329.94	312.4	309.78
Experimental results [K]	728	725	743	751	321	338	317
Relative error	0.003	0.059	0.052	0.071	0.028	–0.076	–0.023

The second validation task was to validate the optimal sealed baffle height which was obtained by numerical simulation. The sealed baffles were executed on the production-line as presented in fig. 2(b). There were three experimental cases:
– Case 1. no sealed baffle, fig. 2(a),
– Case 2. at a baffle height of 1.2 m, and
– Case 3. at a baffle height of 2 m, fig. 2(b).

Table 3 lists the average monitoring temperatures under the three cases. In the experimental study, the nickel-chrome and nickel-silicon *K*-type thermocouples and the temperature sensors were used to measure the plate temperature when the alloying process was working normally.

Table 3. Average monitoring temperatures under the three cases

Experimental cases	Temperature at entrance of fixed soaking zone [K]	Temperature at exit of fixed soaking zone [K]
Case 1. No sealed baffle	752.3	764.2
Case 2. Baffle height of 1.2 m	800.5	992.4
Case 3. Baffle height of 2 m	1030.3	1118.6

Following the installation of the sealed plate, which had a size of about 2.0 m × 0.6 m, the exit temperature of the soaking zone exhibited 46.3% enhanced as compared to the unsealed case. Therefore, the installation of side plates to seal some partial openings at the cooling tower without increasing heating power significantly improved the plate temperature in the soaking zone, thereby characterizing it as an energy-efficient technique for production.

Conclusions

Hot-dip galvanized sheet is an important source of automobile shell material. The alloying temperature is an important parameter that affects the properties of galvanized products. In production, lower or mid-range temperatures of soaking zone deter the achievement of heat preservation for the alloy steel plate, thereby requiring the proposal of an effective method to solve this technical problem. Based on flow pattern and heat transfer mechanisms, a high efficiency technique which consisted of the addition of side sealed baffles at the junction of the cooling tower and soaking zone of the galvanizing kettle was executed to reduce heat dissipation. The technique made the steel sheet temperature improved within the soaking zone without increasing the required heat power, thereby characterizing it as an energy conservation technique.

The temperature distributions of the steel plate and air-flow field in the vertical alloying furnace were analyzed by CFD at Richardson numbers between $1.91 \cdot 10^5$ to $6.30 \cdot 10^5$. When $Ri = 2.4 \cdot 10^5$, the steel plate reached its highest heat absorption and maximal temperature due to the balance between natural and forced convection. Meanwhile, the temperature curve of the plate in the alloying furnace met the requirements for hot galvanizing production. The experiments validated 46.3% increase in the outlet temperature of the soaking zone with 2 m high side sealed baffles as compared to those without baffles.

Acknowledgment

This work was supported by the Natural Science Key Foundation of Hubei Province, China under Contract No. D20171105.

References

[1] Li, Y., Chen, G. Y., Relevent Equipments of Hot Galvanization Technology and Continuous Annealing Furnace, *Heat Treatment Technology and Equipment*, *3* (2010), 012
[2] You, Y., et al., An Investigation in the Effects of Recycles on Laminar Heat Transfer Enhancement of Parallel-Flow Heat Exchangers, *Chemical Engineering and Processing Process Intensification*, *70* (2013), Aug., pp. 27-36
[3] You, Y., *et al*., A Numerical Study on the Turbulent Heat Transfer Enhancement of Rodbaffle Heat Exchanger with Staggered Tubes Supported by Round Rods with Arc Cuts, *Applied Thermal Engineering*, *76* (2015), Feb., pp. 220-232
[4] EI-Kaddah, N., Natarajan, T. T., An Optimal Method for 3-D Numerical Simulation of Electromagnetic Induction Heating Processes, *Proceedings*, Int. Sci. Colloquium Modelling for Electromagnetic Processing, Hannover, Germany, 2008, pp. 51-58
[5] Veranth, J. M., *et al*., Numerical Modelling of the Temperature Distribution in a Commercial Hazardous Waste Slagging Rotary Kiln, *Environmental Science and Technology*, *31* (1997), 9, pp. 2534-2539
[6] Mastorakos, E., *et al*., The CFD Predictions for Cement Kilns Including Flame Modelling, Heat Transfer and Clinker Chemistry, *Applied Mathematical Modelling*, *23* (1999), 1, pp. 55-76
[7] Moon, S., Hrymak, A. N., Scheduling of the Batch Annealing Process – Deterministic Case, *Computers and Chemical Engineering*, *23* (1999), 9, pp. 1193-1208
[8] Sekhar, Y. R., *et al*., Nanofluid Heat Transfer under Mixed Convection Flow in a Tube for Solar Thermal Energy Applications, *Environmental Science and Pollution Research*, *23* (2016), 10, pp. 9411-9417
[9] Rana, P., Bhargava, R., Numerical Study of Heat Transfer Enhancement in Mixed Convection Flow Along a Vertical Plate with Heat Source/Sink Utilizing Nanofluids, *Communications in Non-Linear Science and Numerical Simulation*, *16* (2011), 11, pp. 4318-4334
[10] Biswas, G., *et al*., Computation of Laminar Mixed Convection Flow in a Channel with Wing Type Built-in Obstacles, *Journal of Thermophysics and Heat Transfer*, *3* (2015), 4, pp. 447-453
[11] Sreenivasulu, B., Srinivas, B., Mixed Convection Heat Transfer from a Spheroid to a Newtonian Fluid, *International Journal of Thermal Sciences*, *87* (2015), Jan., pp. 1-18
[12] Ajmera, S. K., Mathur, A. N., Experimental Investigation of Mixed Convection in Multiple Ventilated Enclosure with Discrete Heat Sources, *Experimental Thermal and Fluid Science*, *68* (2015), Nov., pp. 402-411
[13] Yang, G., *et al.*, Flow Reversal and Entropy Generation Due to Buoyancy Assisted Mixed Convection in the Entrance Region of a 3-D Vertical Rectangular Duct, *International Journal of Heat and Mass Transfer*, *67* (2013), Dec., pp. 741-751
[14] Dritselis, C. D., *et al*., Buoyancy-Assisted Mixed Convection in a Vertical Channel with Spatially Periodic Wall Temperature, *International Journal of Thermal Sciences*, *65* (2013), Mar., pp. 28-38
[15] Saleem, M., *et al*., Mixed Convection Flow of Micropolar Fluid in an Open Ended Arc-Shape Cavity, *ASME J. Fluids Eng*., *134* (2012), 9, pp. 91-101
[16] Sharma, N., *et al*., Mixed Convection Flow and Heat Transfer Across a Square Cylinder under the Influence of Aiding Buoyancy at Low Reynolds Mumbers, *International Journal of Heat and Mass Transfer*, *55* (2012), 9-10, pp. 2601-2614
[17] Garoosi, F., *et al*., Two-Phase Simulation of Natural-Convection and Mixed Convection of the Nanofluid in a Square Cavity, *Powder Technology*, *275* (2015), May, pp. 239-256
[18] Patil, P. M., *et al.*, Influence of Convective Boundary Condition on Double Diffusive Mixed Convection from a Permeable Vertical Surface, *International Journal of Heat and Mass Transfer*, *70* (2014), Mar., pp. 313-321
[19] Mehrizi, A., *et al*., Mixed Convection Heat Transfer in a Ventilated Cavity with Hot Obstacle: Effect of Nanofluid and Outlet Port Location, *International Communications in Heat and Mass Transfer*, *39* (2012), 7, pp. 1000-1008
[20] Mahmoodi, M., Mixed Convection Inside Nanofluid Filled Rectangular Enclosures with Moving Bottom Wall, *Thermal Science*, *15* (2011), 3, pp. 889-903
[21] Coussirat, M., *et al*., Computational Fluid Dynamics Modelling of Impinging Gas-Jet Systems, I. Assessment of Eddy Viscosity Models, *ASME J. Fluids Eng*., *127* (2005), 4, pp. 691-703
[22] Coussirat, M., *et al*., Computational Fluid Dynamics modelling of Impinging Gas-Jet Systems, II. Application an Industrial Cooling System Device, *ASME J. Fluids Eng*., *127* (2005), 4, pp. 704-713
[23] Mathews, R. N., Balaji, C., Numerical Simulation of Conjugate, Turbulent Mixed Convection Heat Transfer in a Vertical Channel with Discrete Heat Sources, *International Communications in Heat and Mass Transfer*, *33* (2006), 7, pp. 908-916

[24] Deng, Q. H., *et al*., Fluid, Heat and Contaminant Transport Structures of Laminar Double-Diffusive Mixed Convection in a 2-D Ventilated Enclosure, *International Journal of Heat and Mass Transfer*, *47* (2004), 24, pp. 5257-5269
[25] ***, ANSYS CFX User Guide, Ansys Inc., 2016
[26] ***, ANSYS ICEM CFD User Guide, Ansys Inc., 2016
[27] Mei, D., *et al*., Numerical Simulation of Mixed Convection Heat Transfer of Galvanized Steel Sheets in the Vertical Alloying Furnace, *Applied Thermal Engineering*, *93* (2016), Jan., pp. 500-508

Paper submitted: January 5, 2018
Paper revised: May 4, 2018
Paper accepted: June 7, 2018